S_1-State Internal Conversion of Isolated Azulene Derivatives

Yasushi Numata, Satoru Toyoshima,† Katsuhiko Okuyama,* Masafumi Yasunami, and Isamu Suzuka

Department of Materials Chemistry and Engineering, College of Engineering, Nihon University, Koriyama 963-8642, Japan

Received: September 4, 2008; Revised Manuscript Received: June 28, 2009

The S_0-S_1 hole-burning spectra of azulene and its derivatives, 1-methyl, 2-methyl, 4-methyl, 1-cyano, and 2-cyanoazulenes, were measured under the isolated condition in order to gain an insight into the internal-conversion mechanism. The width of every 0−0 band was dependent on its transition energy and independent of the density of the S_0-state vibrational levels isoenergetic to its zero level of the S_1 state. On the contrary, the vibronic-band broadening of each molecule progressed in proportion to the vibrational excess energy of the S_1 state. In the low-energy region, widths gradually increased, which is attributed to the normal internal conversion. A drastic increase was observed in the medium-energy region in azulene and three methyl derivatives but not in the two cyano ones. This is considered to be the onset of the relaxation process due to the conical intersection suggested by Bearpark et al. [*J. Am. Chem. Soc.* **1996**, *118*, 169]. Anomalous width behavior was found for two vibronic bands whose widths were still narrow even above the onset. One was $0 + 2659$ cm^{-1} band of azulene, that had been already reported by Ruth et al. [*Phys. Chem. Chem. Phys.* **1999**, *1*, 5121], and we could reproduce it by the hole-burning method. Another was $0 + 2878$ cm^{-1} band of 2-methylazulene. This is the vibronic selectivity in competition between the relaxation process and the normal internal conversion. The amplitude vectors of these modes were similar, including the in-plane bending of the CH bond and the stretching of the transannular bond.

Introduction

It has been a half century since Beer and Longuest-Higgins found that azulene is the exception to Kasha's rule.[1] At that time, it was already suggested that an adiabatic crossing between the S_0- and S_1-states potentials induced the fast internal conversion.

The measurement of the population-decay rate is essential to elucidation of a molecular dynamical process.[2−9] In solution, Rentzepis reported the S_1-state lifetime of 7 ps by the picosecond pump-to-probe experiment.[2] Foggi et al. estimated it to be 1.4 ps by femtosecond transient-absorption measurements.[9] Under the isolated condition, Amirav et al.[10] and Suzuki et al.[11] reported a zero level lifetime of 0.8 ± 0.2 and 1.0 ps, respectively, from the measurement of the bandwidth. The full-CI optimization with the CAS6/4−31G and CAS6+GVB/6-31G* calculation performed by Beapark et al. suggested the existence of a conical intersection at 1−13 kcal/mol from the bottom of the S_1-state potential.[12] According to their expectations, Ruth et al. found a sudden increase in the vibronic-band broadening in the region of the vibrational excess energy of more than $0 + 2177$ cm^{-1} by measuring the cavity-ring-down absorption.[13] Zewail's group reported a S_1-state lifetime of 900 ± 100 fs at ~2000 cm^{-1} vibrational excess energy using femtosecond resolved mass spectrometry in a molecular beam.[14]

The introduction of a substituent on the azulene skeleton causes a perturbation of the electronic driving force of the internal-conversion process. The study of the internal conversion by using azulene derivatives was first done by Steer's group. They measured the S_1-state lifetime of azulene derivatives, 2-chloro, 1,4-dimethyl-7-isopropyl, and 4,6,8-trimethylazulenes, in several solvents by the pump-to-probe method.[6,7] Although they could not change the pumping wavelength and control the vibrational excess energy in the S_1 state for the derivatives, they found the relationship between the internal-conversion rate and the transition energy.

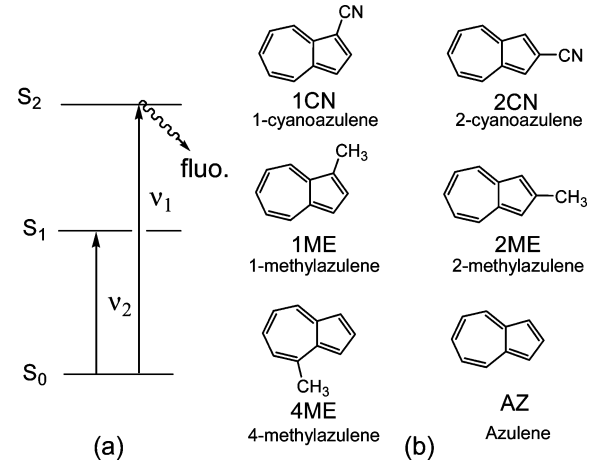

Figure 1. (a) Schematic diagram of hole-burning spectroscopy; (b) Azulene and derivatives.

In this work, in order to gain an insight into the internal-conversion mechanism of the S_1-state of isolated azulene, we measured the vibronic resolved spectra for several derivatives under the jet condition by means of the hole-burning technique. As shown in Figure 1a, the depletion of the S_0-state population due to ν_2-pumping and then to fast internal conversion was measured by monitoring the fluorescence intensity from the S_2 state. For azulene (AZ) and each derivative, 1-cyanoazulene (1CN), 2-cyanoazulene (2CN), 1-methylazulene (1ME), 2-me-

* Corresponding author. E-mail: okuyama@chem.ce.nihon-u.ac.jp.
† Present address: Excel Technology Japan.

10.1021/jp8078502 CCC: $40.75
Published on Web 08/06/2009

thylazulene (2ME), and 4-methylazulene (4ME) in Figure 1b, we observed the width of vibronic transitions in the vibrational excess energy up to 3000 cm^{-1} of the S_1 state. The width of every 0−0 band increased with decreasing transition energy, indicating that the internal-conversion rate was independent of the density of S_0 levels isoenergetic to the 0^0 level of the S_1 state. It was also found that the vibronic band broadening progressed proportionally with the vibrational excess energy of the S_1 state for all derivatives. The drastic increase in the broadening was observed in azulene and the three methyl derivatives but not in the two cyano derivatives.

Experimental Section

The supersonic jet apparatus used in this study is the same as that described elsewhere.[15] The bandwidth of the vibronic transition depends not only on the fast decay process but also on the rotational temperature in the jet. In order to secure identical cooling conditions, the sample temperature (120 °C), the stagnant He pressure (5 atm), and the distance to the crossing point of the jet and the laser beam (12 mm) were identical for all derivatives.

In the measurement of the hole-burning spectra, a frequency doubled dye laser (Continuum, Jaguar, dyes of Styryl 7 and Pyridine 1) pumped by the second harmonics of a YAG laser (Continuum, Powerlite 8010) was used as the probe laser (ν_1), and a fundamental of the dye laser (Spectra Physic PDL-II) pumped by the second harmonics of another YAG laser (Continuum Powerlite 8000, dyes of Styryl 8, Styryl 7, Pyridine 1, DCM, R-101, R-G and R-6G) was used as the pump laser (ν_2). The laser radiation had a typical bandwidth of 0.2 cm^{-1}. Wavelength calibration was carried out by the simultaneous observation of atomic lines of Ar or Ne discharged inside a hollow-cathode lamp (Hamamatsu, L2783−26AR-FE). The ν_1 and ν_2 lasers were coaxially introduced into the vacuum chamber, and the two beams crossed at the jet downstream by 12 mm. The temporal delay of ν_1 and ν_2 was controlled by a digital pulse generator (Stanford Research DG535), and the ν_2 was introduced 50 ns prior to the ν_1. In order to avoid saturation of the vibronic transitions, care was taken in adjusting a suitable laser power of the ν_2 in the range where the dip depth changed linearly depending on the laser power. The laser power of the ν_2 was kept constant while scanning the ν_2 wavelength. To remove scattering light, the fluorescence was detected with a photomultiplier (Hamamatsu R-928) through a monochromator (Nalumi 0.75 m). The fluorescence signal was averaged with a boxcar integrator (Stanford Research, SR250) and recorded on chart paper.

Azulene, 1-cyanoazulene, 2-cyanoazulene, 1-methylazulene, 2-methylazulene, and 4-methylazulene were synthesized and purified according to the method of Yasunami et al.[16]

Ab initio calculations were carried out with Gaussian 03.[17] Optimized structures and vibrational frequencies of all derivatives were obtained through the B3LYP/6-31G(d) level. The density of levels of the S_0 state for each derivative was calculated using the Haarhoff equation.[18]

Results and Discussion

1. S_1−S_0 Hole-Burning Spectra of Azulene Derivatives. The transition diagram is schematically shown in Figure 1a. The ν_1 wavelength is fixed at the 0−0 band in the S_2−S_0 electronic transition for each derivative and the induced fluorescence from the S_2 state is monitored. The fluorescence intensity is proportional to the population of the initial level of the transition, that is, the zero level of the S_0 state. The pump laser, ν_2, is irradiated 50 ns prior to the ν_1 and scanned in the region of the S_1−S_0 electronic transition. When the energy of the scanning ν_2 laser is coincident with a vibronic level of the S_1 state, absorption occurs from the zero-level of the S_0 state. The depletion of the population of the zero level makes the fluorescence intensity decrease. The hole-burning spectrum of the S_1−S_0 electronic transition is obtained by scanning the ν_2 wavelength while monitoring the fluorescence intensity. This is identical with the S_0-S_1 electronic absorption spectrum for the jet-cooled azulene derivative.

According to the uncertainty principle in quantum mechanics, a fast temporal dephasing of the eigenstate results in energetic broadening. The relationship between the uncertainty of time and energy in wavenumber and picosecond units is

$$\Delta t\,(\mathrm{ps}) \cdot \Delta E\,(\mathrm{cm}^{-1}) \geq 5.3\ \mathrm{cm}^{-1} \cdot \mathrm{ps}$$

The fast internal conversion of the S_1-state azulene derivatives diffuses the vibronic level. The supersonic jet provides the collision-free and ultracooled condition that makes it possible to observe vibronic transitions with large widths due to the fast internal-conversion process. In our hole-burning spectra in the S_1−S_0 transition, we observe vibronic bands with widths of 3.5−35 cm^{-1}. Under the identical jet condition, vibronic bands in the S_2−S_0 transition are observed with a width of 1.4−3.8 cm^{-1} which is produced by rotational contour and intramolecular vibrational redistribution (IVR). Since the contribution to the S_0-S_1 bandwidth due to rotational contour and IVR is the same extent of that in the S_0-S_2 band, the extra width of the S_0-S_1 transition is ascribed to the S_1-state fast internal conversion. From the uncertainty principle, the width in the S_1−S_0 transition, therefore, corresponds to 0.4−5.9 molecules ps^{-1} as the internal-conversion rate.

In this manuscript, we present the effect of substituents on the internal-conversion rate. A substituent makes a significant perturbation on the electronic driving force of the internal-conversion process.[19] Targets are shown in Figure 1 b. As an electronic character of the substituent in the S_0 state, a cyano group strongly withdraws electrons from the aromatic ring, whereas a methyl group is a weak electron donor. On the azulene skeleton, the π-electron density on the 1-carbon is largely different from that on the 2-carbon. According to the calculation by Beapark et al., the conical intersection between the S_0 and the S_1 states was located on the skeleton coordinates of azulene. We expect the substituent to influence the energy position of the intersection and the internal-conversion rate.

The S_1−S_0 hole-burning spectra of 1CN, 2CN, 1ME, 2ME, and 4ME are shown in Figure 2. The longitudinal axis is the intensity of the fluorescence from the S_2-0^0 level with a maximum value of 100. The prominent band with the lowest energy is assigned as the 0−0 band because no bands are observed lower in energy for at least 1000 cm^{-1}. The transverse axis is the wavenumber relative to the 0−0 band to which the position for each derivative is vertically aligned. The 0−0 band energies of 1CN, 2CN, 1ME, 2ME, and 4ME are observed at 14 807, 14 274, 13 415, 14 793, and 14 652 cm^{-1}, respectively. These transition energies are in ascending order as follows: 1ME < 2CN < 4ME < 2ME < 1CN. Even at the 0^0 level, broadening due to internal conversion occurs for all derivatives. The width of 1ME is largest among these molecules because of its lowest transition energy. Details will be discussed later.

The spectral features of the vibronic structure in all spectra resemble that of azulene. In all derivatives, the appearance of the unambiguous 0−0 band indicates no large changes in

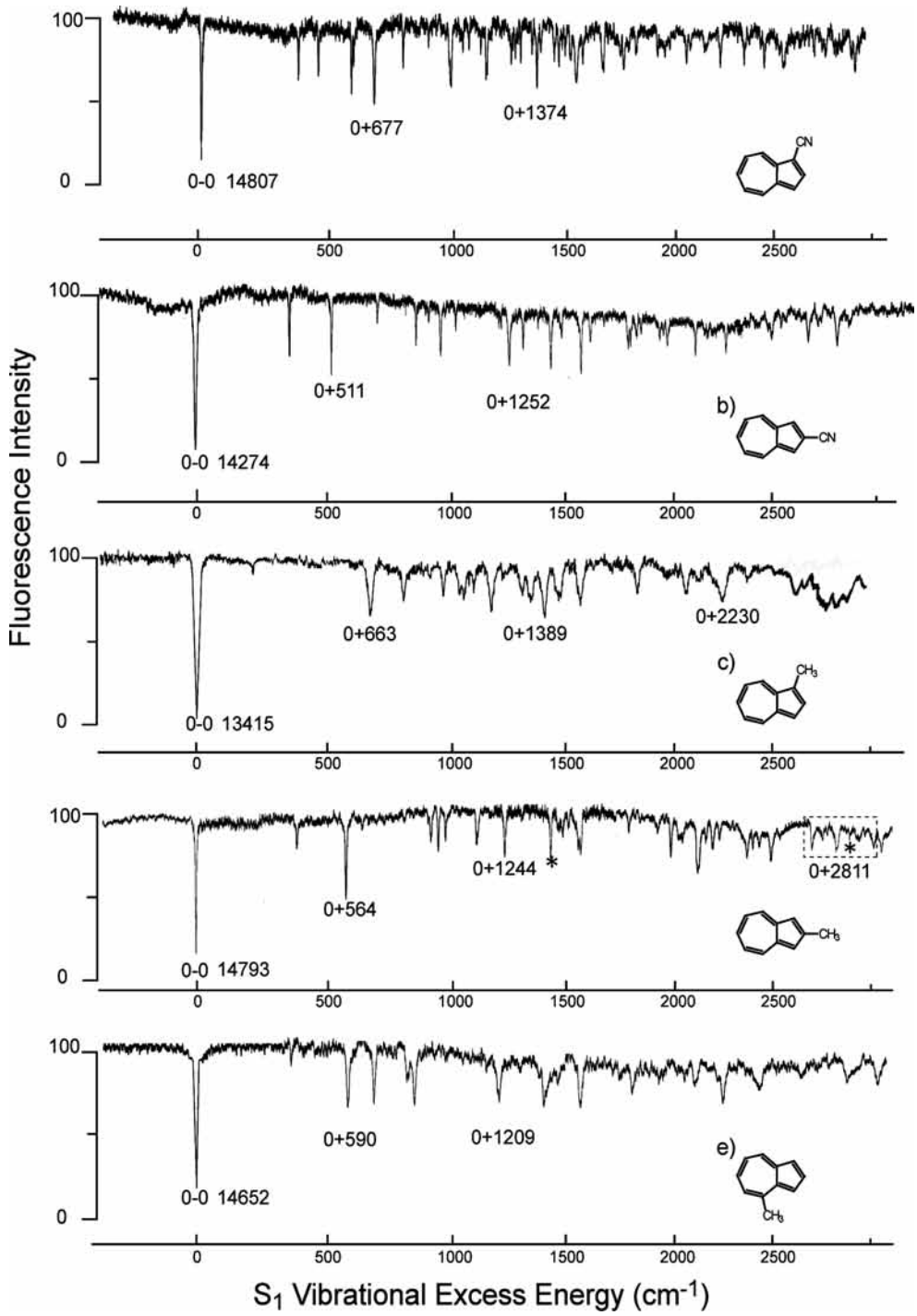

Figure 2. S_1-S_0 hole-burning spectra: (a) 1CN, (b) 2CN, (c) 1ME, (d) 2ME, and (e) 4ME.

structure upon excitation. In the spectra, the bands commonly seen at ~670 cm^{-1} for 1-substituted and at ~500 cm^{-1} for 2-substituted derivatives correspond to the ν_{16} skeletal vibrational mode of azulene. Intense bands between 1200 and 1400 cm^{-1} are also skeletal modes. The active appearance of skeletal modes means that excitation to the S_1 state slightly deforms the azulene framework.[20]

2. Energy and Width of the 0−0 Band of the S_0-S_1 Transition. Table 1 shows the transition energy, the width of the 0−0 band of the S_0-S_1 transition, and the relative density of S_0-state vibrational levels isoenergetic to the 0^0 level of the S_1 state. In addition to the molecules in Figure 1b, values measured for 2PH (2-phenylazulene), 6PH (6-phenylazulene),[21] and guaiazulene (1,4-dimethyl-7-isopropylazulene)[22] are shown in the table. Two stable conformers were found in guaiazulene,[23] indicated as GUA and GUB. Figure 3 shows the least-squares-fitting curve (solid line) of the 0−0 bandwidths versus their transition energies. It is noted from the table and Figure 3 that the width has a simple relationship to the transition energy. The width smoothly decreases with an increase in the transition energy.

The uncertainty principle states that the width gives the lower limit of the lifetime (Δt), of which the reciprocal is the internal-conversion rate (k) from the S_1 state to the S_0 state. On the basis of Fermi's golden rule, the internal-conversion rate under the collision free condition is proportional to the product of the square of the electronic factor (β^2), the Franck−Condon factor (F), and the density of the S_0-state vibrational levels (ρ). The

TABLE 1: Transition Energy and Width of the 0-0 Band

molecules	transition energy (cm^{-1})	width[c] (cm^{-1})	density of levels[d]	$(\rho_{0+2500})/(\rho_{0-0})$[e]	slope[f] × 10^3
1ME	13 415	11.7	166	45	3.7
GUB[a]	13 417	11.7			
GUA[a]	13 671	10.4			
6PH[b]	14 019	8.0			
2CN	14 274	5.0	61	34	1.8
AZ	14 283	5.6	1	28	2.0
2PH[b]	14 533	4.3			
4ME	14 652	4.5	1510	40	2.1
2ME	14 793	3.5	1270	41	2.2
1CN	14 807	3.5	117	31	1.8

[a] GUA and GUB indicate the two conformational isomers of guaiazulene (1,4-dimethyl-7-isopropylazulene) described in ref 23. [b] PH is phenylazulene in ref 21. [c] Widths are measured as the full width at the half of the dip minimum in wave numbers. [d] The density of S_0-state vibrational levels isoenergetic to the 0^0 level of the S_1 state is calculated by Haarhoff's method.[18] Values in the column are relative to that of azulene. The absolute value of azulene is 1.5×10^{12} levels cm. [e] This is a ratio of the density of levels at 0 + 2500 cm^{-1} to that at the 0° level of the S_1 state. [f] The slope represents the increment of the width (cm^{-1}) against the S_1-state vibrational excess energy (cm^{-1}), corresponding to the solid line of each plot in Figure 6.

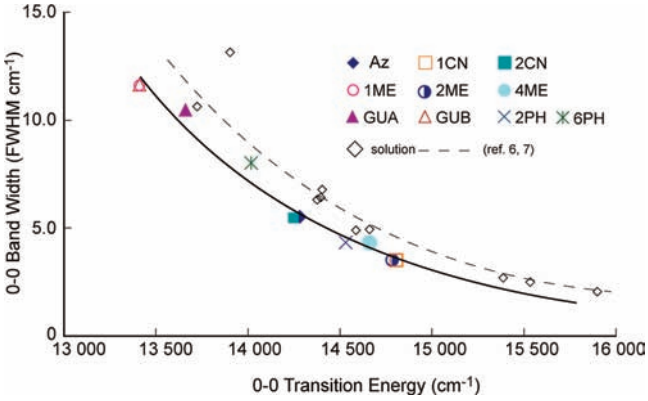

Figure 3. Transition energy and width of 0−0 bands for azulene derivatives. The plot in the isolated condition is represented by the solid line, and the dashed line is that reported in solution by Steer's group.[6,7]

density of the S_0-state levels isoenergetic to the 0^0 level of the S_1 state for each derivative is calculated by Haarhoff's method.[18] Values in the table are relative to that of azulene. The absolute value is 1.5×10^{12} levels cm. With an increase in the number of atoms constituting the derivative, the number of normal modes increases, and the density of levels also increases. As seen from the table, there is, however, no relationship between the width and the density. The density of 4ME, for instance, is 1510 times larger than that of azulene whereas its width is smaller.

Next, we will consider the *F*. Klessinger and Michl described the Franck−Condon factor in the Fermi's golden rule as follows:[24] If the energy difference between the two states is large, as is generally the case for the S_0 and S_1 states, the zero vibrational wave function ($v' = 0$) of the S_1 state overlaps with a higher vibrational wave function of the S_0 state in a region close to the equilibrium geometry, where the kinetic energy of the nuclear motion is large and the value of the wave function is small. The overlap integral is therefore close to zero and the Franck−Condon factor makes the transition very unlikely. Since we can make similar discussions with respect to the *F*, it is not an effective factor to the internal conversion. Furthermore, as we will describe in the next section, we found that the bandwidth gradually increased with increasing the vibrational excess energy and no irregular behavior of bandwidths against vibrational modes could be observed. Since the *F* includes the wave function of the S_1-state vibronic level, a significant dependence on modes should be seen if the *F* was effective. Consequently, we conclude the *F* is not a dominant factor in the internal conversion.

Finally, we will discuss an electronic factor. As mentioned above, we observed the simply increasing bandwidths with increasing the vibrational excess energy, indicating that the dominant factor should be effective in the overall electronic state. Therefore, the electronic factor is the most important in the internal-conversion process since neither the density of states nor the Franck−Condon factor are unambiguously effective to the internal-conversion rate at the 0−0 band.

In solution, Steer et al. reported the picosecond pump-to-probe experiment for azulene derivatives.[6,7] However, they could not select the 0−0 band nor control the pumping level because the pumping-laser-wavelength was fixed. A width calculated from their decay rate is added to Figure 3 and the least-squares-fitting curve is depicted as a dashed line. Taking into account the fact that the width of the solid line we measured includes the rotational contour, we found that the curvature in the isolated condition agrees well with that in solution. This indicates that the effect of solvent on the internal-conversion rate is quite small and that the intramolecular factor also dominates over the environmental one.

3. Dependence of the Width on the Vibrational Excess Energy. As a representative case of this research, we will discuss the results of 2ME. The enlargement of the spectrum in the 0−0 band at 14793 cm^{-1} is shown in Figure 4a. The profile is a nicely symmetrical Lorentzian indicating homogeneous broadening due to fast decay and also indicates no saturation concerning the laser intensity, molecular concentration in the jet, or the data acquisition system. The width of 3.5 cm^{-1} gives us a lifetime of 3.1 ps under the assumption that the rotational contour width is 1.8 cm^{-1}, which is the 0−0 band of the S_2-S_0 electronic transition observed under the identical jet condition. The lifetime is three times longer than that of azulene reported by Amirav et al.[10] and Suzuki et al.[11] The plotting point of 2ME is located at the lower right position in Figure 3. The transition energy of the 0−0 band of 2ME is 510 cm^{-1} higher than that of azulene.

If the determining factor of the internal-conversion rate depends only on the transition energy, then the width of the vibronic band with a certain vibrational excess energy should be smaller than that of the 0−0 band. Figure 4b,c shows vibronic bandwidths with vibrational excess energies of 0 + 1244 cm^{-1} and 0 + 2811 cm^{-1} of 2ME, respectively. Beyond our expectations, the width becomes much larger with an increase in the vibrational excess energy. The width of the 0 + 2811 cm^{-1} band is 6.7 times larger than that of the 0−0 band. Bandwidths of all vibronic bands are plotted in Figure 5. The error range, determined by several measurements, becomes larger depending on the decrease in the intensity of the vibronic band. The features in the figure can be classified into three parts. In the low energy region from the 0−0 band to 2700 cm^{-1}, the width gradually increases as shown by a solid line. The medium energy region from 2700 to 2800 cm^{-1} shows a steep increase. In the high energy region over 2800 cm^{-1}, the width becomes very large but there is no change. The behavior of the change in widths is quite similar to that of azulene reported by Ruth et al.,[13] but the onset energy of the steep increase is different. We

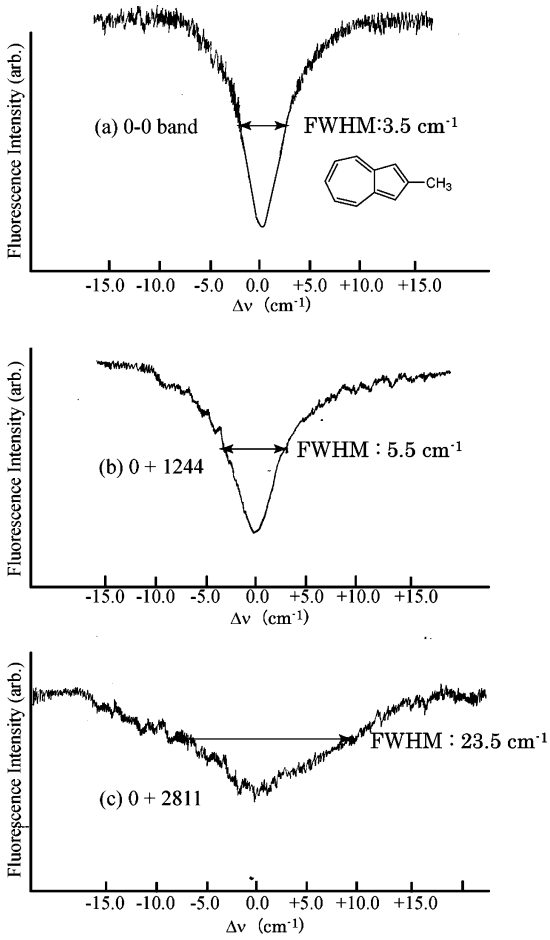

Figure 4. Expanded spectra of 2ME: (a) 0−0 at 14793 cm^{-1}, (b) 0 + 1244 cm^{-1}, and (c) 0 + 2811 cm^{-1}.

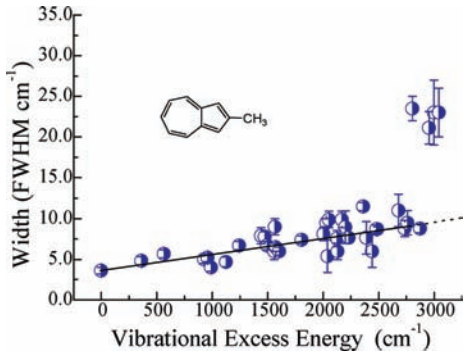

Figure 5. Dependence of the width on the vibrational excess energy in the S_1 state of 2ME.

observe the onset of 2ME at 2700 cm^{-1} and that of azulene is reported at 2100 cm^{-1}. Ruth et al. remarked on two anomalous vibronic bands at 0 + 2659 and 0 + 2877 cm^{-1} whose widths were still narrow even above the steep rise, and the vibronic selectivity of the internal-conversion rate was discussed. We also observe a similar phenomenon in 2ME and will discuss it later.

Figure 6 represents the dependence of the bandwidth on the vibrational excess energy for other derivatives including that of azulene, which we measured by the hole-burning method. This is almost identical with that reported by Ruth et al. For all derivatives, the common phenomenon is that widths in the low energy region gradually broaden with increasing excess energy. The remarkable difference is the presence of the steep rise of the width. Onsets are observed for azulene and the three methyl derivatives in the medium energy region. For cyano derivatives, such a rise is not observed, and the width increases linearly to ∼3000 cm^{-1}.

Ruth et al. reported a rise at ∼2100 cm^{-1} in azulene coinciding with the energy of the conical intersection predicted by Bearpark et al.[12] and concluded that the steep rise was induced by the intersection. Their discussion was made with only respect to this point. Before discussing the conical intersection, we propose the possibility of IVR within the S_1 state. Fujii et al. reported the onset of the IVR in the S_2 state at 1980 cm^{-1}.[25] Vibrational frequencies of the S_2 state are not so different from those of the S_1 state that the onset of the IVR in the S_1 state is similar to that in the S_2 state. The energy of the steep rise coincides with the onset of not only the conical intersection but also the IVR. The derivatives have a different IVR onset, which could be estimated by the density-of-levels calculation for the S_1 state. The comparison for the derivatives would lead to the solution. Table 2 shows the observed steep-rise energy and the calculated IVR onset energy for our targets. The vibrational density of levels of azulene at the IVR onset is calculated to be 10 ± 4 levels cm. The vibrational excess energy with the identical density for derivatives was calculated. Methyl derivatives have nine more normal modes than azulene, in which the internal rotation of the methyl group is often flexible and makes a large contribution to the density of levels. The IVR onset of methyl derivatives is relatively low. Cyano derivatives are rigid molecules with three more normal modes than azulene, and IVR onsets were calculated to be 1650 cm^{-1}. As seen from the table, the energy of the steep rise of widths has no correlation with the estimated onset energy of the IVR. We conclude that the steep rise of the internal-conversion rate is induced by other factors than IVR. Clearer insights will be possible from quantum-chemistry calculations on the derivatives at the same level performed by Bearpark et al.

On the other hand, we find a correlation between the steep-rise energy and the π-electron density on the azulene skeleton in the S_1 state. Table 2 includes the relative π-electron densities of the azulene ring in the S_0 and the S_1 states calculated by the extended Hückel molecular orbital (MO) method. In the S_0 state, a cyano group is well-known as a strong electron withdrawing group, and a methyl group is a weak electron donor. The former has a large positive value, and the latter has a small negative one. Values of the S_0 state do not explicitly correspond to the steep-rise energy. The transition of a π electron to the lowest antibonding π orbital, however, makes the electron distribution on the azulene skeleton change slightly. The π-electron density of the S_1 state has good correspondence to the steep-rise energy. For example, π-electron densities of methyl derivatives are slightly different from those of azulene and the steep-rise energies of these molecules maintain this order. Cyano derivatives have a largely positive π-electron density in the S_1 state and their steep-rise regions are expected to be higher than the region we observed. To support this, we present the results from guaiazulene (GUA: 1,4-dimethyl-7-isopropylazulene). The steep-rise energy of GUA is observed at 1450 cm^{-1}, the lowest among the derivatives we studied, and its π-electron density is the smallest in the table. Even though our calculation is very simple, we get good correspondence between the steep-rise energy and the π-electron density on the azulene skeleton in the S_1 state.

The width in the low energy region increases linearly as shown by a solid line in Figure 6. The observed increment of the slope is listed in the right column of Table 1. As seen from the table, there is good correlation between the slope and the calculated increment of density of levels of the S_0 state, which

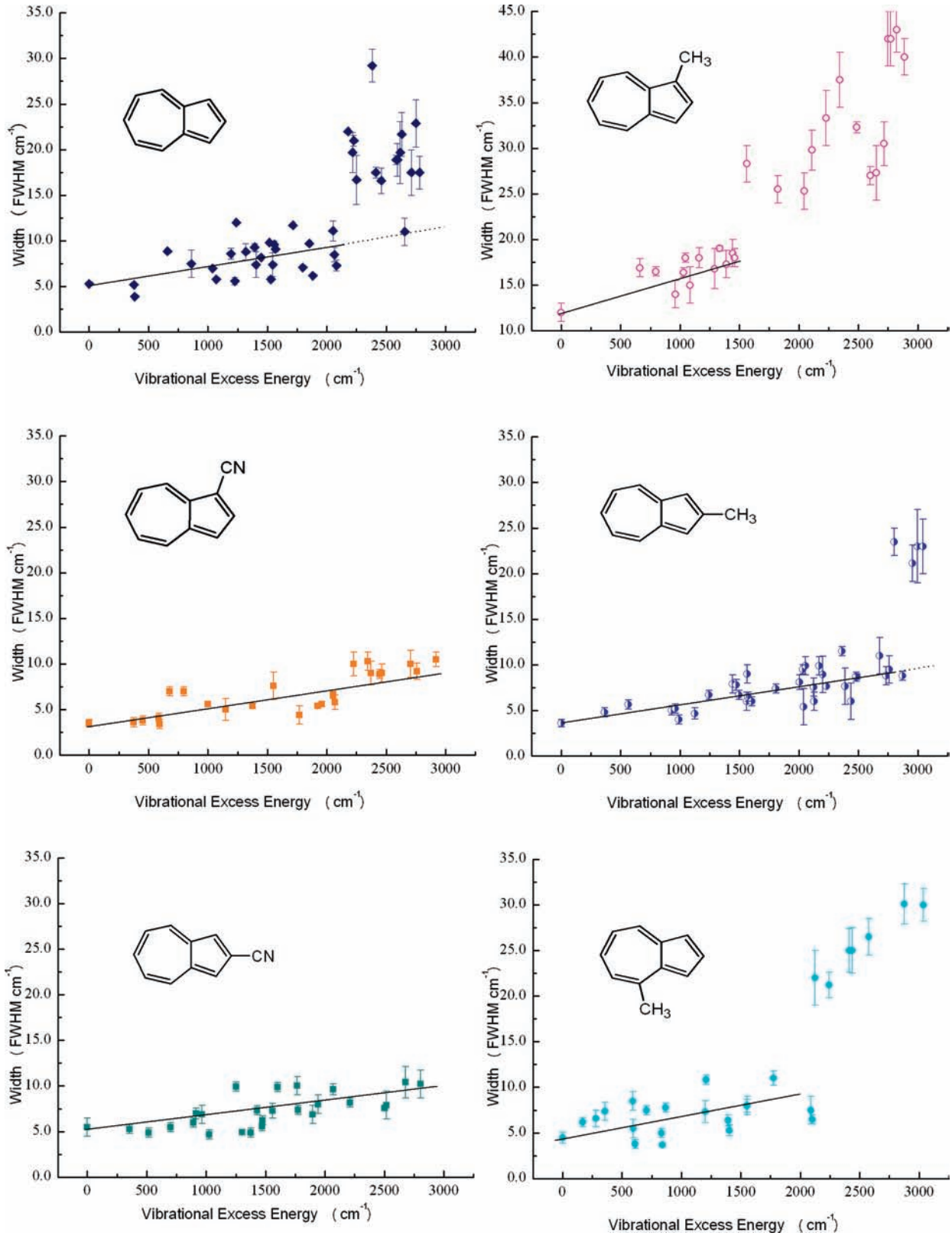

Figure 6. Dependency of bandwidths on the vibrational excess energy for azulene and derivatives.

appears as ρ_{0+2500}/ρ_{0-0} in Table 1. Methyl derivatives with high density increments have a large slope relative to cyano derivatives. The bandwidth in the low energy region is determined by the density of states of the S_0 state, indicating that the increase of bandwidths is due to normal internal conversion. It is, therefore, concluded that the internal-conversion rate inside an electronic state is attributed to the density of vibrational levels of the S_0 state while the overall S_1 state is determined by the electronic factor dominating over the factor of the density.

As mentioned above, Ruth et al. observed two anomalous vibronic bands of azulene at $0 + 2659$ and $0 + 2877$ cm^{-1} whose widths were still narrow even over the steep rise. They performed cavity-ring-down absorption spectroscopy, which has the high ability of the detection sensitivity. This enables the

TABLE 2: Steep-Rise Energy for Azulene Derivatives

molecules	steep-rise energy	estimated IVR onset[a]	relative π-electron density[b] S_0 state	relative π-electron density[b] S_1 state
GUA	1450		0.0430	−0.0820
1ME	1500	1500	−0.0045	−0.0320
Az	2100	1980	0	0
4ME	2200	1550	−0.0090	+0.0030
2ME	2700	1650	−0.0110	+0.0017
2CN	>3000	1650	0.2600	+0.4500
1CN	>3000	1650	0.3200	+0.3100

[a] IVR onsets for derivatives are calculated where the vibrational excess energy reaches the density of the S_1-state vibrational levels of $\rho = 10 \pm 4$ levels cm, whose value corresponds to the IVR onset of the S_2-state azulene. [b] The π-electron density means the Mulliken charge on the azulene skeleton for derivatives, which is calculated by the extended Hückel MO method. Values in the column are relative to that of azulene.

detection of a small amount of an impurity having an absorption near the wavelength region, for example, an azulene derivative originating in the synthetic process. On the other hand, hole-burning spectroscopy has a high selectivity for the research object by the selective excitation of the ν_1. We re-examined the result of Ruth et al.[13] by the hole-burning method and the dependency of widths of azulene is presented in the top left in Figure 6. As a result, we can also reproduce the identical phenomenon at $0 + 2659$ cm^{-1}, but the unambiguous narrowing at $0 + 2877$ cm^{-1} could not be observed. Moreover, we could observe another vibronic band with a narrow width over the steep rise in 2ME at $0 + 2878$ cm^{-1} with a width of 8.8 cm^{-1}. Besides these, no vibronic bands with similar behaviors were observed in our targets. The spectra enlarged around $0 + 2878$ cm^{-1} in 2ME and near $0 + 2659$ cm^{-1} in azulene are shown in Figure 7a,b, respectively. We carefully measured the spectra in this region several times. Figure 7 is one of them. In Figure 7a, two bands at 2680 cm^{-1} and 2733 cm^{-1} seem broad, but we confirmed by several time measurements that each band consists of two narrow width bands: 9.0 cm^{-1} and 12.0 cm^{-1} widths at 2680 cm^{-1} and 8.8 cm^{-1} and 9.5 cm^{-1} widths at 2733 cm^{-1}. The band at 2811 cm^{-1} has a width of 23.5 cm^{-1} as shown in Figure 4c. The onset of the steep rise for 2ME lies between the bands at 2733 and 2811 cm^{-1}. The band at 2878 cm^{-1} has a narrow width of 8.8 cm^{-1} over the steep rise. As seen from Figure 6, widths of two vibronic bands can be extrapolated from the solid line determined in the low energy region. This clearly indicates the vibronic selectivity in the process inducing the sudden increase of widths as was previously pointed out by Ruth et al.[13] The findings presented here support their results.

We attempted to assign the two vibrational levels to normal modes. Vibrations with frequencies of 2659 cm^{-1} of azulene and that of 2878 cm^{-1} of 2ME must be the first overtones because quantum-chemistry calculations of the normal-coordinate frequency indicate no fundamental modes in the frequency range between 1700 and 3000 cm^{-1}. In the spectrum of 2ME in Figure 2d, the vibronic band appears at $0 + 1440$ cm^{-1}, which is a reasonable frequency as the fundamental of the 2878 cm^{-1} overtone. It is highly probable in azulene derivatives that the totally symmetric mode is Franck−Condon active since deformation upon $\pi\ \pi^*$ excitation should occur to preserve the molecular plane. The integrated intensities of $0 - 0$, $0 + 1440$, and $0 + 2878$ cm^{-1} bands are 1.00, 0.37, and 0.16, respectively. The intensity distribution is also reasonable as a typical progression. Abou-Zied et al. carried out the normal coordinate analysis of 2ME by means of the single-vibronic-level dispersed fluorescence spectrum in the jet and by an ab initio method.[26] The vibration with the frequency of 1453 cm^{-1} in the S_0 state

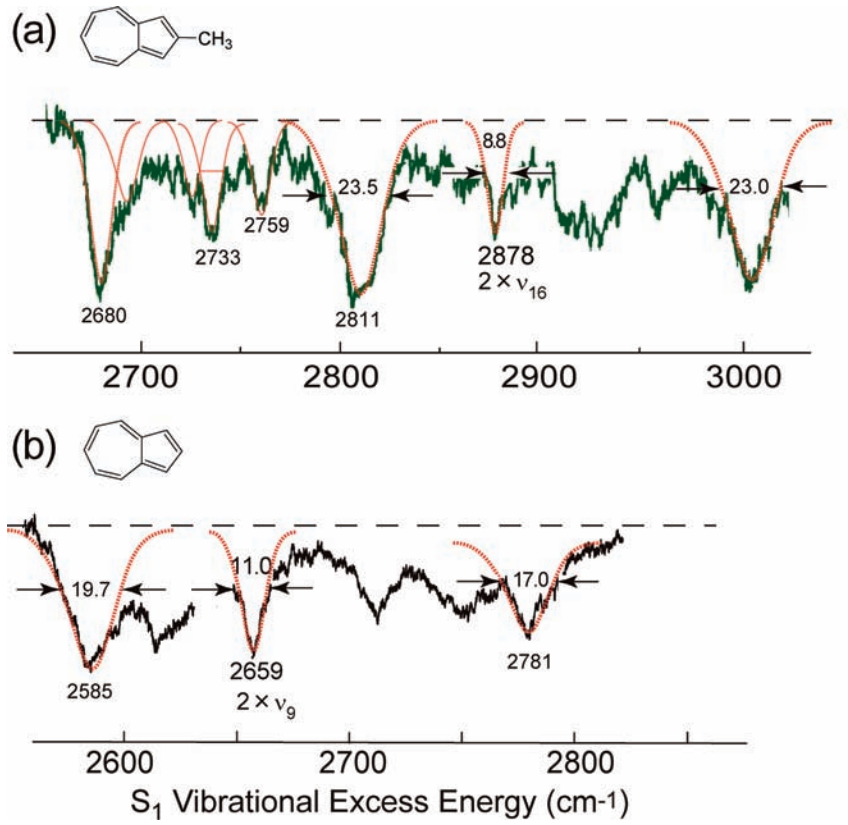

Figure 7. S_1-S_0 hole-burning spectra enlarged around (a) $0 + 2878$ cm^{-1} in 2ME and (b) $0 + 2659$ cm^{-1} in azulene.

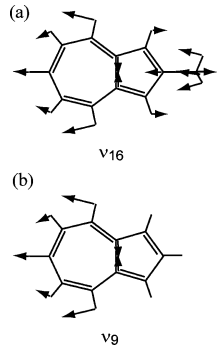

Figure 8. Displacement vectors for (a) ν_{16} of 2ME and (b) ν_9 of azulene.

was assigned to the totally symmetric ν_{16} which is attributed to in-plane CCH bending. From the symmetry and the similarity in the frequency, we assign the 1440 cm^{-1} vibration to ν_{16} of the S_1 state. The displacement vector appears in Figure 8a. In a similar way, the 2659 cm^{-1} vibration of azulene can be assigned to the totally symmetric $2 \times \nu_9$ and of the S_1 state. Displacement vectors are shown in Figure 8b. These are similar to each other.

4. Internal Conversion and the Conical Intersection. From our findings, we conclude that the diffuseness of the 0−0 band and the vibronic bands in the low energy region of azulene derivatives is attributed to a normal internal conversion according to Fermi's golden rule. The sudden increase in widths observed in azulene and its methyl derivatives cannot, however, be explained only by the normal internal conversion. A similar phenomenon in cyano derivatives should occur at a higher energy region than we observed, since our observation was restricted to the active Franck−Condon region. Calculations performed at the same level as Bearpark et al. on the derivatives could support an adiabatic transition such as a conical intersection. A high-level quantum-chemistry calculation could also clarify the relationship between the onset energy and the π-electron density on the azulene skeleton.

It is interesting to find that vibronic selectivity in competition between the normal internal conversion and the conical intersection induced the sudden increase of widths. Figure 8 shows that ν_{16} of 2ME and ν_9 of azulene have similar vectors in the amplitudes of each atom. These modes include the relatively large CH bending and do not induce large skeletal deformation. Bearpark et al. proposed a large skeletal deformation upon the excitation to the S_1 state together with the conical intersection. This means that the skeletal deformation readily interconnects the intersection with the high probability. In general, the bands which appeared in the $\pi-\pi^*$ transition spectrum are almost the skeletal vibration. Most of the bands in the hole-burning spectra in this study are also skeletal vibration, which induced the skeletal deformation. Then the fast nonradiative process occurs. On the other hand, since the modes as shown in Figure 8 include the relatively large CH bending and do not induce large skeletal deformation, the fast nonradiative process leading to the conical intersection does not occur. We expect that the bandwidth of vibronic states of CH stretching vibration which have excess vibrational energy of over 3000 cm^{-1} can be narrow. In fact, Fiedler found a few bands with bandwidths <15 cm^{-1} in a high energy region of azulene.[27] These bands may be assigned to the vibrational modes which do not induce large skeletal deformation.

Conclusion

The S_0-S_1 hole-burning spectra of azulene and its derivatives, 1-methyl, 2-methyl, 4-methyl, 1-cyano, and 2-cyanoazulenes, were measured under the isolated condition. The 0−0 bandwidth of the derivatives increased with decreasing transition energy, indicating that the internal-conversion rate was dependent on the electronic factor rather than the density of vibrational levels in the S_0 state. It also was discovered for all derivatives that the vibronic band broadening progressed proportionally to the vibrational excess energy of the S_1 state. The increase of the bandwidths in the low-energy region is considered to be due to normal internal conversion because the observed slope had a close relationship to the calculated increment of the density of levels in the S_0 state. A drastic increase of bandwidth was observed in azulene and the three methyl derivatives but not in the two cyano ones. We interpret the drastic change in the bandwidths as the conical-intersection onset that had been predicted by Bearpark et al. In addition to the $0 + 2659$ cm^{-1} band of azulene, we found an anomalous vibronic band at $0 + 2878$ cm^{-1} of 2-methylazulene, whose width was still narrow even over the onset. This indicated that the vibronic selectivity is in competition between the processes of the conical intersection and the normal internal conversion. Both vibronic bands are assigned as the overtones of the totally symmetric CCH in-plain bending including stretching of the transannular bond.

Acknowledgment. The authors thank Dr. O. Takahashi for very valuable discussions on the calculation of the π-electron density of azulene derivatives. We thank Ms. Mitsumoto and Mr. Katayama for their experimental assistance. This research was supported by a grant from Nihon University.

References and Notes

(1) Beer, M. B.; Longuest-Higgins, H. C. *J. Chem. Phys.* **1955**, *23*, 1390–1391.
(2) Rentzepis, P. M. *Chem. Phys. Lett.* **1968**, *2*, 117–120.
(3) Hochstrasser, R. M.; Li, Y. Y. *J. Mol. Spectrosc.* **1972**, *41*, 297–301.
(4) Ippen, F. P.; Shank, C. V.; Woerner, R. L. *Chem. Phys. Lett.* **1977**, *46*, 20–23.
(5) Schwarzer, D.; Troe, J.; Schroeder, J. *Ber. Bunsen-Ges. Phys. Chem.* **1991**, *95*, 932–934.
(6) Tittelbach-Helmrich, D.; Wagner, B. D.; Steer, R. P. *Chem. Phys. Lett.* **1993**, *209*, 464–468.
(7) Wagner, B. D.; Szymanski, M.; Steer, R. P. *J. Chem. Phys.* **1993**, *98*, 301–307.
(8) Wurzer, A. J.; Wilhelm, T.; Piel, J.; Riedle, E. *Chem. Phys. Lett.* **1999**, *299*, 296–302.
(9) Foggi, P.; Neuwahl, F. V. R.; Moroni, L.; Salvi, P. R. *J. Phys. Chem. A* **2003**, *107*, 1689–1696.
(10) Amirav, A.; Jortner, J. *J. Chem. Phys.* **1984**, *81*, 4200–4205.
(11) Suzuki, T.; Ito, M. *J. Phys. Chem.* **1987**, *91*, 3537–3542.
(12) Bearpark, M. J.; Bernardi, F.; Clifford, S.; Olivucci, M.; Robb, M. A.; Smith, B. R.; Vreven, T. *J. Am. Chem. Soc.* **1996**, *118*, 169–175.
(13) Ruth, A. A.; Kim, E.-K.; Hese, A. *Phys. Chem. Chem. Phys.* **1999**, *1*, 5121–5128.
(14) Diau, E. W.-G.; Feyter, S. D.; Zewail, A. H. *J. Chem. Phys.* **1999**, *110*, 9785–9788.
(15) Okuyama, K.; Numata, Y.; Odawara, S.; Suzuka, I. *J. Chem. Phys.* **1998**, *1097*, 7185–7196.
(16) Yasunami, M.; Miyoshi, S.; Kenegae, N.; Takase, K. *Bull. Chem. Soc. Jpn.* **1993**, *66*, 892–899.
(17) Frisch, M. J.; Trucks, G. W.; Schlegel, H. B.; Scuseria, G. E.; Robb, M. A.; Cheeseman, J. R.; Montgomery, J. A., Jr.; Vreven, T.; Kudin, K. N.; Burant, J. C.; Millam, J. M.; Iyengar, S. S.; Tomasi, J.; Barone, V.; Mennucci, B.; Cossi, M.; Scalmani, G.; Rega, N.; Petersson, G. A.; Nakatsuji, H.; Hada, M.; Ehara, M.; Toyota, K.; Fukuda, R.; Hasegawa, J.; Ishida, M.; Nakajima, T.; Honda, Y.; Kitao, O.; Nakai, H.; Klene, M.; Li, X.; Knox, J. E.; Hratchian, H. P.; Cross, J. B.; Bakken, V.; Adamo, C.; Jaramillo, J.; Gomperts, R.; Stratmann, R. E.; Yazyev, O.; Austin, A. J.; Cammi, R.; Pomelli, C.; Ochterski, J. W.; Ayala, P. Y.; Morokuma, K.; Voth, G. A.; Salvador, P.; Dannenberg, J. J.; Zakrzewski, V. G.; Dapprich, S.; Daniels, A. D.; Strain, M. C.; Farkas, O.; Malick, D. K.; Rabuck, A. D.;

Raghavachari, K.; Foresman, J. B.; Ortiz, J. V.; Cui, Q.; Baboul, A. G.; Clifford, S.; Cioslowski, J.; Stefanov, B. B.; Liu, G.; Liashenko, A.; Piskorz, P.; Komaromi, I.; Martin, R. L.; Fox, D. J.; Keith, T.; Al-Laham, M. A.; Peng, C. Y.; Nanayakkara, A.; Challacombe, M.; Gill, P. M. W.; Johnson, B.; Chen, W.; Wong, M. W.; Gonzalez, C.; Pople, J. A. *Gaussian 03, Revision C.02*; Gaussian, Inc.: Wallingford, CT, 2004.

(18) Haarhoff, P. C. *Mol. Phys.* **1963**, *7*, 101–117.

(19) Lee, A. M. D.; Coe, J. D.; Ullrich, S.; Ho, M.-L.; Lee, S.-J.; Cheng, B.-M.; Zgierski, M. Z. *J. Phys. Chem.* **2007**, *111*, 11948–11960.

(20) Okuyama, K.; Mikami, N.; Ito, M. *J. Phys. Chem.* **1985**, *89*, 5617–5625.

(21) Okuyama, K.; Numata, Y.; Masuda, T.; Shimada. M. *J. Phys. Chem. A*; preparation for submitting.

(22) Numata, Y.; Motousu, M.; Okuyama, K.; Suzuka, I. *J. Phys. Chem. A*; preparation for submitting.

(23) Carrabba, M. M.; Woudenberg, T. M.; Kenny, J. E. *J. Phys. Chem.* **1985**, *89*, 4226–4230.

(24) Kleissinger, M.; Michl, J. In *Excited states and photochemistry of organic molecules*; VCH Publishers, Inc.; New York, 1995; Chapter 5, pp 257−260.

(25) Fujii, M.; Ebata, T.; Mikami, N.; Ito, M. *Chem. Phys.* **1983**, *77*, 191–200.

(26) Abou-Zied, O. K.; Sinha, H. K.; Steer, R. P. *J. Mol. Spectrosc.* **1997**, *183*, 42–56.

(27) Fiedler, S. E.; Hoheisel, G.; Ruth, A. A.; Hese, A. *Chem. Phys. Lett.* **2003**, *382*, 447–453.

JP8078502